jove

Direct Force Measurements of Subcellular Mechanics in Confinement using Optical Tweezers

Frederic Català-Castro[1], **Valeria Venturini**[2,3], **Santiago Ortiz-Vásquez**[1], **Verena Ruprecht**[2,4], **Michael Krieg**[1]

[1] Neurophotonics and Mechanical Systems Biology, Institut de Ciències Fotòniques, ICFO [2] Center for Genomic Regulation (CRG), The Barcelona Institute of Science and Technology [3] Institut de Ciències Fotòniques, ICFO [4] Universitat Pompeu Fabra (UPF)

Corresponding Authors

Verena Ruprecht
verena.ruprecht@crg.eu
Michael Krieg
michael.krieg@icfo.eu

Citation

Català-Castro, F., Venturini, V., Ortiz-Vásquez, S., Ruprecht, V., Krieg, M. Direct Force Measurements of Subcellular Mechanics in Confinement using Optical Tweezers. *J. Vis. Exp.* (), e62865, doi:10.3791/62865 (2021).

Date Published

August 30, 2021

DOI

10.3791/62865

URL

jove.com/t/62865

Abstract

During the development of a multicellular organism, a single fertilized cell divides and gives rise to multiple tissues with diverse functions. Tissue morphogenesis goes in hand with molecular and structural changes at the single cell level that result in variations of subcellular mechanical properties. As a consequence, even within the same cell, different organelles and compartments resist differently to mechanical stresses; and mechanotransduction pathways can actively regulate their mechanical properties. The ability of a cell to adapt to the microenvironment of the tissue niche thus is in part due to the ability to sense and respond to mechanical stresses. We recently proposed a new mechanosensation paradigm in which nuclear deformation and positioning enables a cell to gauge the physical 3D environment and endows the cell with a sense of proprioception to decode changes in cell shape. In this article, we describe a new method to measure the forces and material properties that shape the cell nucleus inside living cells, exemplified on adherent cells and mechanically confined cells. The measurements can be performed non-invasively with optical traps inside cells, and the forces are directly accessible through calibration-free detection of light momentum. This allows measuring the mechanics of the nucleus independently from cell surface deformations and allowing dissection of exteroceptive and interoceptive mechanotransduction pathways. Importantly, the trapping experiment can be combined with optical microscopy to investigate the cellular response and subcellular dynamics using fluorescence imaging of the cytoskeleton, calcium ions, or nuclear morphology. The presented method is straightforward to apply, compatible with commercial solutions for force measurements, and can easily be extended to investigate the mechanics of other subcellular compartments, e.g., mitochondria, stress-fibers, and endosomes.

Introduction

Tissue morphogenesis is a complex process in which biochemical signals and physical forces are spatiotemporally coordinated. In the developing embryo, gradients of biochemical signaling factors dictate fate specification and ensure correct tissue patterning[1,2]. At the same time, intrinsic and extrinsic forces play a role in building the architecture of the embryo[3,4]. The influence of cell cortex mechanics in this context has been studied extensively[5,6]. The tight interconnection between mechano-chemical processes during morphogenesis relies on the properties of single cells to sense and respond to mechanical forces in their tissue microenvironment. Cells, thereby decode mechanical signals *via* the presence of force-sensitive subcellular and molecular elements that transduce mechanical information into specific signaling pathways controlling cell behavior, cell fate, and cell mechanics.

A hallmark of developmental processes is that cells organize as groups to build multicellular structures. As such, single cells rarely rearrange and move alone but are associated in a tight sociotope in which they show collective behavior such as supracellular migration[7], (un)jamming transitions[8,9] or blastocyst compaction[10]. Mechanical forces generated within and between cells serve as important cues to instruct collective cell dynamics[7,11]. But even when cells move alone, such as progenitor cells that squeeze their way between tissue sheets or narrow tissue niches, they experience extensive anisotropic mechanical forces when navigating a three-dimensional environment. These mechanical stresses on cells have profound consequences on cellular behavior[12,13]. Several mechanisms have been investigated that converge on the nucleus as a major mechanotransduction element[14,15], as passive or active mechanical element during migration within a dense 3D tissue environment[15,16].

We recently proposed a mechanism that equips cells to measure shape deformations using the nucleus as an elastic intracellular mechano-gauge[12]. The nucleus, being the largest organelle in a cell, undergoes large deformations when cells polarize, migrate, or change their shape under mechanical stretch, confinement, or osmotic stress[16,17,18,19]. We found that nuclear envelope stretch along with the intracellular positioning of the nucleus provides cells with information on the magnitude and type of cell deformation (such as cell compression versus cell swelling). Stretching of the nucleus is associated with an unfolding of the inner nuclear membrane (INM), which promotes calcium-dependent cPLA2 (cytosolic phospholipase A2) lipase activity at the INM followed by the release of Arachidonic Acid (AA) and rapid activation of myosin II at the cell cortex. This leads to increased cell contractility and amoeboid cell migration above a threshold of cortical contractility[6]. The mechanosensitive response to cell deformation occurs in less than a minute and is reversible upon confinement release, suggesting that the nucleus acts as a strain gauge for cellular proprioception regulating adaptive cell behavior under mechanical stress conditions. This mechanosensitive pathway is shown to be active in progenitor stem cells derived from zebrafish embryos, both in pluripotent and lineage-committed cells[12] and is conserved in different species and cell lines[20].

In addition to the nuclear properties as a cell-mechanosensor, nuclear architecture and mechanics are intrinsically regulated during development and in response to cell fate specification[21], hence tuning cellular mechano-

sensitivity[22,23]. The consequence might be a change in nuclear compliance that allows for morphological changes and transitions from a premigratory to a migratory state and vice versa[8].

Several techniques to measure cell nucleus mechanics have been applied, such as atomic force microscopy[24,25], micropipette aspiration[26,27], microfluidic technology[28], and microneedles[29]. However, many of these techniques are invasive in the sense that the entire cell must be deformed, limiting the measurement of mechanical characteristics and force-dependent responses of the nucleus itself. To circumvent the simultaneous deformation of the cell surface and its mechanosensitive cell cortex[30], isolated nuclei were studied in various contexts[31,32]. However, it cannot be ruled out that nuclear isolation is associated with a change in mechanical nucleus properties and their regulation (reference[24] and own unpublished observations).

Optical tweezers (OTs) are a versatile technology that has allowed a plethora of experiments in cell mechanobiology and have been instrumental in our understanding of how molecular machines convert chemical into mechanical energy[33,34]. Optical tweezers use a tightly focused laser beam to exert optical forces onto dielectric particles that have a refractive index higher than the surrounding medium[33]. Such forces can be of the order of hundreds of pico-Newtons and result in effective confinement of the particle within the laser trap focus, enabling manipulation of the trapped particle in three dimensions. The use of light has an important advantage in that the measurement can be performed non-invasively inside living cells. Optical manipulations are further limited to the trap focus of the laser beam. Hence, the manipulation can be performed without stimulating the surrounding cellular membranes and does not perturb the actin cortex or mechanosensitive processes at the plasma membrane, such as the force-dependent activation of ion channels.

The difficulty of the optical tweezer approach is to precisely determine the forces applied to the microsphere using classical approaches that rely on indirect force calibration based on the equipartition theorem or the use of defined Stokes-drag forces to measure a laser-power dependent escape force[35]. Whereas these methods are straightforward to implement in an *in vitro* experiment, they usually cannot be translated into a cellular environment. Several strategies have been introduced into the field that rely on a direct force calibration, derived from the first principles of momentum conservation[36,37]. Unlike other force spectroscopy approaches, force measurements are deduced from a local interchange of light momentum with the arbitrarily-shaped trapped particle[38,39]. In our experimental set-up, changes in light momentum arising from optical forces are directly measured without the need for *in situ* trap calibration[40,41,42,43]. Thus, the measurements become possible in a viscous environment such as the interior of the cell or even within a tissue, and forces can be readily quantified down to the pN level.

In this protocol, we describe an assay to mechanically manipulate intracellular organelles or structures and quantitatively assess their mechanical properties by an optical tweezer set-up. This set-up is integrated into a spinning disk fluorescent microscope enabling parallel imaging of cellular behavior or intracellular dynamics. The assay allows for the characterization of the mechanical properties of specific cellular compartments, such as the nucleus, while simultaneously studying the possible mechanoresponse and activation of molecular signaling

pathways as a result of the deformation itself. Furthermore, optical trapping of injected microbeads within cells allows for an increase in the indentation force thanks to a considerably higher refractive index of the polystyrene bead (n = 1.59) compared to the intrinsic refractive contrast[44] of the nucleus (n ~ 1.35) versus cytoplasm (n ~ 1.38). The presented strategy can be easily adapted to the study of other intracellular structures and organelles, as well as other approaches involving active microrheology, the use of multiple optical traps to probe the same/different sub-cellular structures simultaneously, and measurements targeting cell mechanobiology in the live embryo.

Protocol

All protocols used have been approved by the Institutional Animal Care and Use Ethic Committee (PRBB-IACUEC) and implemented according to national and European regulations. All experiments were carried out in accordance with the principles of the 3Rs. Zebrafish (*Danio rerio*) were maintained as previously described.

1. Preparation of isolated primary embryonic zebrafish progenitor stem cells

1. Micropipette and agarose preparation

   NOTE: For a complete zebrafish embryo microinjection protocol, see reference[45].

   1. With a micropipette puller, pull a 1.0 mm glass capillary to obtain two needles[45]. Store the unused needles in a 150 mm Petri dish attached to a playdough cushion or in an inside-out lab tape ring to protect the thin tip from damage during transport.
   2. Melt 1% ultrapure agarose in E3 (5 mM NaCl, 0.17 mM KCl, 0.33 mM $CaCl_2$, 0.33 mM $MgSO_4$) in a standard kitchen/lab microwave for 10 s. Heat the mix repeatedly for short periods of time (few seconds) until the agarose melts.
   3. When the agarose is completely melted, let it cool down briefly, and then pour it into a 10 cm Petri dish. Slowly add the triangular microinjection mold (see **Table of Materials**) on the top of the agarose avoiding the appearance of bubbles. Do not push the mold, ensuring it stays on the agarose surface.
   4. When the agarose solidifies completely, remove the triangular mold very slowly by exerting a gentle force to avoid any breaks in the agarose. The plate can be stored upside down at 4 °C for 2-4 weeks.
   5. 30 min before the microinjection, take the plate out of the fridge and add E3 prewarmed to 28 °C to let it stabilize at room temperature.

2. Injection mix preparation

   1. To prepare the injection mixture, dilute 1 µm microbeads (polystyrene, non-fluorescent) in 1:5 ratio in RNase free water.
   2. Prepare mRNA for transient expression of fluorescent markers or expression of recombinant gene constructs and/or co-injection of morpholino at the desired concentration.

      NOTE: A typical injection mixture for the co-injection of microbeads together with 100 pg of mRNA per embryo to label, for example, the nucleus with H2A-mCherry is: 1 µL of beads + 1 µL of mRNA (stock concentration is 1 µg/µL) + 2.5 µL of RNA free water + 0.5 µL of phenol red (stock solution 0.5%, phenol red is not mandatory; it is used for a better visualization of the injected drop but the non-labeled injection drop is also visible for an experienced

experimenter). RNA injection can also be useful to select injected embryos. Fluorescent microbeads can be injected, instead of non-fluorescent, to visualize them.

3. Microinjection needle loading and calibration

    1. Turn on the microinjector using the **Time-Gated** option. This setting is very important to calibrate the injection volume properly. Set the gating time at approximately 500 ms.

    2. Load 3 µL of the injection mixture into the needle using a micro-loader pipette.

    3. Insert the needle into the micromanipulator and seal tightly. Check whether the micromanipulator is in a good position and has enough freedom to move in x-y direction on the injection plate.

    4. Measure the drop size using a micrometer slide (5 mm/100 divisions) with a drop of mineral oil on top[45] and ejecting a drop of the injection mix directly into the mineral oil.

    5. Crop the needle with sharp forceps at a steep angle to generate a sharp pointed tip. Adjust the drop size to 0.1 mm, corresponding to 0.5 nL of injected material.

        NOTE: If by cutting the needle, this volume is exceeded, it is recommended to redo the calibration procedure with a new needle. The gating time of the microinjector can be slightly adjusted to match the drop volume; however, short gating times correspond to a large needle diameter, which potentially damages the embryos.

4. Microinjection of zebrafish embryos at one-cell stage

    1. Collect zebrafish embryos shortly after fertilization for microinjection of the bead mixture directly into the one-cell (zygote) stage embryo before the first cell division occurs.

        NOTE: This ensures proper distribution of microspheres and a high enough yield of isolated blastomeres with at least one microsphere per cell at later developmental stages in which experiments are performed (blastula-gastrula stage). Indentation experiments can still be performed if there are two spheres within the cell, but cells that have no beads should be excluded (even though indentation without spheres is possible). AB wildtype strains were used in this protocol, but any other strain, e.g., TL can be used.

    2. Place one-cell stage embryos (zygote) in a prewarmed triangular-shaped 1% agarose mold, as shown in **Figure 1A**, using a plastic Pasteur pipette.

    3. Remove extra medium with the same pipette to avoid the embryos floating around. Gently push the embryos into the triangular mold *via* a brush. Keep some space in between embryos to facilitate the correct orientation (**Figure 1B**).

    4. Gently align the embryos with a brush so that the embryos are oriented laterally, with the one cell of the zygote being clearly visible, as shown in **Figure 1B**. An ideal orientation for microinjection is reached when the one cell of the embryo is facing the needle direction (injection *via* the animal pole of the embryo) or in the opposite way facing the yolk cell (injection *via* the vegetal pole of the embryo), as shown in **Figure 1C**.

5. Hold the dish with one hand and use the other hand to position the needle tip using the micromanipulator controller. Lower the needle tip toward the embryos.

6. Pierce the chorion and enter the one-cell embryo with the needle while monitoring the procedure through the stereomicroscope. Ensure correct placement of the needle and, after injecting, the correct location of the injected drop as shown in **Figure 1C**.

7. Repeat for all embryos: move the needle up, slide the dish with the embryos until the next embryo is centered, lower the needle, and inject it.

8. Once the entire set of embryos is injected, remove the embryos from the agarose mold/Petri dish by flushing some E3 and put them in a new Petri dish using a plastic Pasteur pipette. It is recommended to place sufficient media on the injection plate to avoid drying out of embryos during the microinjection procedure.

9. Repeat the procedure until the desired number of embryos is injected. Embryos must be at one cell stage to ensure maximal and homogeneous spreading of the beads.
   NOTE: This procedure is optimized for early blastula embryos and likely needs to be optimized if different developmental stages are to be investigated.

10. Place the injected embryos inside an incubator at 28-31 °C for approximately 4 h or until the desired stage (**Figure 1D**) before proceeding with the protocol for primary cell culture.
    NOTE: Optionally, let the embryos develop beyond the blastula stage (or desired measurement time point) to ensure survival and rule out toxicity artifacts. At larval stages, mount anesthetized larvae with tricaine in 0.75% agarose and image the distribution of microspheres in various tissues. To make a stock solution, mix: 400 mg of tricaine powder in 97.9 mL of distilled water, approximately 2.1 mL of 1 M TRIS-base (pH 9), and adjust to pH 7. This solution can be stored at 4 °C. To use tricaine as an anesthetic, dilute 4.2 mL of stock solution in 100 mL of egg's medium (or desired media); in this case, E3 was used. Consult reference[46] for details.

2. Single-cell preparation and staining

1. Place the sphere stage embryos (4 hpf, hours post fertilization) in a glass dish using a plastic Pasteur pipette. Select the embryos that are positive for the signal of the injected beads, and that express the fluorescent protein in case of mRNA injection. Some embryos might show high bead clustering and can be excluded.

   1. Manually dechorionate the embryos using forceps. Transfer approximately 10-15 embryos to 1.5 mL reaction containers using a glass Pasteur pipette.
      NOTE: When the embryos are dechorionated, they attach to the plastic, and the use of glassware is required. As an alternative to the glass plate, a plastic Petri dish with a thin layer of 1% agarose can be used. Manual dechorionation should be preferred over enzymatic Pronase treatment to prevent proteolytic damage to cell surface proteins and potential changes in mechanical cell and tissue properties, preventing extended recovery times[47].

2. Remove the E3 media and add 500 µL of pre-warmed CO_2-independent tissue culture medium (DMEM-F12; with L-glutamine and 15 mM HEPES, without sodium

bicarbonate and phenol red supplemented with 10 units penicillin and 10 mg/L streptomycin).

NOTE: Do not use CO_2-dependent media unless a microscope incubator is used. The use of, e.g., RPMI in carbonate-buffered conditions cause changes in the media's pH and can affect cell survival. Another key aspect is to avoid culture media that contain serum. Serum may contain Lysophosphatidic acid (LPA), a potent activator of the Rho/ROCK pathway, capable of controlling cellular contractility and motility in progenitor stem cells[6]. The osmolarity of the medium should be maintained at 300 mOsm to avoid osmotic challenges that could interfere with nuclear morphology or mechanics[12].

3. Manually dissociate cells by gently shaking the tube. Ensure that the contents of the tube become turbid with no big chunks visible by the eye. Avoid the formation of bubbles to minimize the damage and loss of cells.
4. Centrifuge at 200 x *g* for 3 min. The pellet must be clearly visible.
5. Remove the supernatant and follow one of the steps detailed below.
    1. If no staining is needed, add 500 µL of DMEM. Gently resuspend with a 200 µL pipette by targeting a liquid jet onto the pellet. Do not exert excessive shear force onto the cells. Foaming indicates damage to the cells.
    2. For labeling the nucleus with DNA dyes such as Hoechst, mix 0.5 µL of DNA-Hoechst (stock 2 mg/mL) in 1,000 µL of DMEM to obtain 1 µg/mL of final concentration. Add 500 µL of this staining solution to the cells and resuspend gently. Incubate for 7 min in the dark.
    3. To stain the cells with a fluorescent chemical calcium indicator Calbryte-520, add Calbryte-520 to a 5 µM concentration in DMEM. Incubate for 20 min in the dark.

        NOTE: The protocols indicated in steps 2.5.2 and 2.5.3 have been optimized for these specific products. Other staining can be performed using the protocols indicated by the manufacturer.
6. Centrifuge again using the same settings as in step 2.4; remove the supernatant, and gently resuspend the cells (to avoid the formation of clusters) in 50 µL of DMEM for samples in suspension or 20 µL of DMEM for cells in confinement.

3. Preparation of optical trapping chambers using polydimethylsiloxane (PDMS) spacing

NOTE: Optical force measurements based on light momentum detection require the capture of all the light emerging from the optical traps[40]. For the robustness of the invariant calibration factor α (pN/V), the light distribution at the back focal plane (BFP) of the optical force sensor must bear an accurate correspondence to the photon momentum. This determines the distance from the surface of the collecting lens to the trapping plane to approximately 2 mm, which is the maximum height of the optical trapping chambers.

1. PDMS spin-coating of #1.5 glass bottom dishes.

    NOTE: The following recipe is provided for approximately 40 dishes. The resulting microchamber will have different heights depending on whether experiments are to be conducted on suspended or confined cells (**Figure 1D**).
    1. Mix 9 mL of the base polymer PDMS and 1 mL of PDMS curing agent in a 50 mL conical tube. Mix the

two products actively to ensure proper distribution of the curing agent.

2. Degas the mixture to avoid bubbles using a vacuum pump. Introduce the conical tube in a vacuum bottle and evacuate the chamber. Wait until no bubbles are present in the mixture.
   NOTE: Open the vacuum slowly to prevent foaming and spills of the PDMS out of the falcon tube.
3. Place the glass bottom dish on the spin-coater chuck (**Figure 2A**). Be gentle not to scratch, fingerprint, or get the dish dirty. Protect the spin-coater box from PDMS leaks with aluminum foil.
4. For OT chambers for experiments on cells in suspension, add approximately 250 µL of PDMS mixture at the center of the bottom dish and spin it at 750 rpm for 1 min. The height of the PDMS layer will be 50 µm approximately[48].
5. For OT chambers for experiments on confined cells, add a small drop of PDMS (approximately 50 µL) and spin it at 4,000 rpm for 5 min. The height of the PDMS layer will be 10 µm approximately. For a detailed protocol on how to obtain different PDMS thicknesses, see reference[48].
6. Cure the PDMS-coated glass-bottom dishes at 70 °C for 1 h.
7. Cut a 1 x 1 cm square onto the PDMS layer with a scalpel and peel it off with tweezers (**Figure 2C**). In the case of confined cells, wash PDMS debris with isopropanol.

2. Chamber coating for experiments with lightly attached cells in suspension
   1. Add 100 µL of Concanavalin A (ConA) at 0.5 mg/mL to cover the entire surface of the square cavity and let it incubate for 30 min.
      NOTE: ConA is a lectin that binds to cell surface sugars and couples individual cells onto the coverglass surface.
   2. Remove the ConA drop and rinse the surface carefully with DMEM medium without scratching the ConA treated surface.
   3. Add 30 µL of the previously prepared sample (step 2.6) into the well and gently resuspend to get rid of any cell clusters.
   4. Close the cavity by gently placing a 22 x 22 mm #1.5 cover glass on top of the PDMS rims (avoid letting it fall abruptly, use forceps if possible, **Figure 2B,C**).
      NOTE: Any coverslip thickness would work for the upper glass cover (the collecting lens has a working distance of 2 mm).
3. Chamber preparation for experiments with cells in confinement
   1. Put a 10 µL drop of solution containing cells (step 2.6) into the square cavity (**Figure 2B**).
   2. Very gently, sandwich the sample with a 22 x 22 mm cover glass such that the drop spreads in the entire area and no bubbles are observed. Again, it is convenient to use forceps, as shown in **Figure 2C**, to prevent the cover glass from falling abruptly.

4. Alternative options for OT chamber spacing

NOTE: These steps can be followed if no microfabrication workshop or spin coater is available.

1. Chamber preparation for experiments with cells in suspension

   NOTE: In case no spin coater is available, a spacer can be made using normal, double-sided scotch tape (approximately 100 µm in height).

   1. Cut a piece of double-sided scotch tape with an approximately 10 cm x 10 cm square hole in the center (same dimensions as in PDMS, **Figure 2B**).
   2. Remove one of the protective layers of the tape by peeling it off and place the uncovered side of the tape in the center of a #1.5 H glass-bottom dish. Press gently to get all the surface adhered to the glass while avoiding air bubbles, and then remove the remaining protective layer of the tape by peeling it off.
   3. Follow the instructions in step 3.2.

2. Chamber preparation for experiments with cells in confinement

   NOTE: To precisely confine cells, monodisperse microparticles with a known diameter can be used as spacers between the two cover glasses.

   1. Add 10 µm polystyrene beads to suspended cells at a concentration of 10^4 beads/µL.
   2. Put a 10 µL drop of solution containing cells and beads on a 22 x 60 mm cover glass.
   3. Very gently, sandwich the sample with another 22 x 60 mm cover glass such that the drop spreads in the entire area and no bubbles are observed. To position the upper cover glass gently (avoid that it falls down abruptly), it is convenient to use forceps.
   4. As the sample can dry out, it is recommended to perform the preparation swiftly.

5. Setting up the optical trap for intracellular measurements

NOTE: The following steps are optimized for a commercial optical tweezers platform comprising an optical micromanipulation module based on acousto-optic deflection (AOD) and an optical force sensor based on direct detection of light momentum changes (**Figure 2**, reference[12,40,49]). Details and optical components of the set-up can be found in **Figure 2F**. To observe force-induced deformation during the optical tweezer manipulations, a Nipkow spinning-disk confocal microscope is coupled into the left port of the inverted microscope for dual color fluorescence imaging. Without the lack of generality, this protocol can be applied with any dynamic OTs system equipped with direct force measurements based on light momentum detection. Detailed step-by-step procedures are available to construct homebuilt optical gradient traps for *in vivo* applications[50]. Those based on AOD modulation stand out for eventual experiments with multiple traps and fast measurements[51,52]. Several protocols to construct a light-momentum based instrument exist in the literature[36,39,40,53], and any other imaging modality (differential interference contrast, widefield fluorescence, etc.) can be employed.

1. Optical tweezers start-up
   1. In order to optimize for the output power stability, turn on the laser at considerably high power (e.g., 3 W) at least 30 min before the experiment.
   2. Turn on the electronics module of the optical micromanipulation and force measurement units.

      NOTE: Apply all laser safety measures and only use equipment approved by the institutional board. Never use the eyepieces of the optical microscope when the laser is on. Always use approved IR

protection goggles (OD7 in the 950-1080 nm range), block the IR laser light with the shutter in the epifluorescence port 2, and do not execute the optical trapping software until finishing the optical force sensor alignment after step 5.3. In general, do not use a highly reflective sample, as the back-reflection could cause damage to the laser.

3. Control the trap power with the rotating HWP (**Figure 2F**) at the entrance of the optical micromanipulation module.

   NOTE: The commercial optical micromanipulation module used in this protocol already incorporates this feature. For homebuilt optical trapping systems, integrate this tool for power control so that higher and more stable laser powers can be used.

2. Use an empty microchamber for calibration

   1. Cut a 1 x 1 cm square onto a double-sided scotch tape and attach it onto a 1 mm thick microscope slide.

   2. Add water into the square and close it from the top with a #1.5 cover glass (22 x 22 mm). Adding a slightly higher volume of water, e.g., 30-40 µL is advised to avoid bubbles inside the covered chamber. Wipe the calibration chamber gently in case of water spilling out of it.

3. Alignment of the optical force sensor

   1. Put a droplet of water on the 60x/1.2 water immersion objective. Place the calibration chamber on the stage with the #1.5 cover glass facing the objective. Focus onto the lower surface, where the cell samples will eventually be.

   2. Add a droplet of immersion oil on top of the upper glass slide covering the sample (**Figure 2D**). Lower the collecting lens of the force sensor unit carefully until it contacts the oil droplet.

      NOTE: The droplet must be large enough so that it covers the whole lens that collects the laser light emerging from the traps. Usually, 200 µL is sufficient to cover the entire surface and provide a stable immersion contact. Be conservative and avoid overfilling as it might leak into the sample.

   3. Following the manufacturer's protocol for the optical force sensor alignment, look at the sample plane image on the auxiliary camera that will be used to position the OTs (AUX, **Figure 2F**). Very gently, lower the optical force sensor until the field stop (FS, **Figure 2F-G**) appears conjugated onto the sample plane. This will ensure proper direct force measurements from sample-invariant detection of light momentum changes[40].

      NOTE: Close the FS enough so that its image becomes smaller than the field of view (FOV), hence, visible. Be extra careful and do not push the collecting lens of the optical force sensor against the sample. The vertical position of the optical force sensor can alternatively be determined from analysis of the trapping light distribution at the BFP for light cones with defined numerical aperture (NA).

   4. Ensure that there are no air bubbles in the oil droplet; these can directly affect the force measurements. To check for air bubbles, put the Bertrand lens in place (BL, **Figure 2G**) and observe the imaging path through the eyepiece. If any dirt or air bubbles are visible or more oil is needed (**Figure S1A**), clean the lens and chamber with dust-free lens tissue and repeat the procedure in steps 5.3.2 and 5.3.3. An unobstructed optical path is depicted in **Figure S1B**.

5. Using the lateral screws placed on the holder of the optical force sensor, center the FS into the FOV. For accuracy, open the FS so that it almost fills the FOV visible on the auxiliary camera (AUX, **Figure 2F**).

6. Optical tweezer optimization

NOTE: The direct force measurement relies solely on the change of light momentum arising from the force exerted onto the trapped particle, and thus, in contrast to indirect methods, trap stiffness does not need to be calibrated prior to each experiment. The instrument-specific conversion of deflection/force factor (α; pN/V, reference[41]) is calibrated by the manufacturer and is thus experiment invariant. However, because the laser spot is manipulated over an area of 70 µm x 70 µm, steps 6.2-6.5 are critical to ensure optimal trapping and power stability. The following steps are supplied in the manufacturer software so that the OTs get optimized over the working area in a semi-automatic way.

1. Launch the OTs software and the acquisition software for camera AUX.
2. Subtract the initial voltage baseline by clicking on the **Step 1: Electronics Offset** step in the System Calibration submenu of the optical tweezers driving software.
3. To perform trap power flattening across the OT working area, set the trap power to half of its maximum by rotating the HWP accordingly. Do not change the trap power by changing the laser output, but with the rotating HWP (**Figure 2F**). Click on **Step 2: Power** to initiate the automated routine for trap power flattening.
   NOTE: This is a critical step to compensate for variation of the trap power across the OTs working area (**Figure S1D**). A successful routine brings trap power variation down to 2% across the OTs working area and converges after 2 min.
4. To perform trap position calibration, remove the IR filter so that the light from the laser is visible on the camera. Find the IR spot by setting the image plane focused onto the lower surface of the microchamber. Obtain the smallest IR spot possible by tuning the image plane (objective position) and the histogram contrast in camera AUX acquisition software. If needed, reduce the power of the optical trap by rotating the HWP (**Figure 2F**). Click on **Step 3: Position** to start the automated routine or trap positioning calibration.
   NOTE: This routine enables the precise correspondence of the OT's position coordinates in camera AUX to the AOD steering angles. A successful routine generates the angle-to-position mapping in several seconds.
5. Initial momentum compensation
   NOTE: The movement of the optical trap across the sample causes variations in the light-momentum distribution at the BFP (**Figure S1E, F**). This leads to force-independent signal changes related to laser position over the working area, even though the trap power has been flattened as in step 6.3. The consequence is a variation in force baseline due to position (independent of an actual force acting on the optically-trapped bead) that needs to be corrected prior to each experiment.
   1. Set the trap power that will be used in the experiments, by rotating the HWP (**Figure 2F**).
   2. Click on the **Global Offset** option in the **Tools** submenu. This will open the **Offset Cancel** assistant of the optical tweezers software that corrects the initial momentum baseline.

3. Click on **Offset | Compensate** to correct the position-variant initial momentum.

   NOTE: If no modification affects the optical path during the ongoing weeks, the trap power flattening (step 6.3) and position (step 6.4) maps will remain invariant. We hence recommend to always use the same combination of optical elements (dichroic mirrors, filters, etc.) that may affect the laser trap path or to carry out a new trap power flattening routine. Regarding the initial momentum compensation (step 6.5), the manufacturer of the OTs platform provides an on-the-fly calibration that must be changed for every new trapping power and experimental session. Steps 6.3 and 6.4 must be carried out on the empty calibration slide described in step 5.2. In a sample containing cells or other objects, step 6.5 should be carried out free of objects that may alter light scattering in the OTs working area.

6. Optionally, trap a microsphere and move the trap at a known velocity while recording the force signal. For example, set the trap to perform a triangular oscillation: the recorded force signal will be a square signal.

   NOTE: The force value should increase linearly with the velocity, according to the drag force acting on the bead. This test serves as a positive control that force measurements are being undertaken correctly[38]. Alternatively, the optical force sensor can be used to obtain the optical trapping stiffness, κ [pN/μm], and the position calibration factor, β [μm/V], from power spectral analysis[35]. Under correct alignment, the invariant calibration factor provided by the manufacturer is $\alpha = \kappa \cdot \beta$ [pN/V].

1. Initiate a real time force reading by clicking on Plot 1 in the Measures submenu in the manufacturer software. This will provide a reading of the current optical trapping force and power.
2. Open the **Oscillation Parameters** dialog from the **Tools** submenu. Set a triangular-space waveform shape in the Shape and Type selector rings, respectively. As an example, set an amplitude of 10 μm and a frequency of 3 Hz. This will result in a viscous force of approximately 1 pN onto a microbead with a diameter of 1 μm[38].
3. On the camera's AUX window, right-click on the microbead and select **Start Oscillating**. The force reading will become a square force signal with plateaus at ±1 pN.
4. Right-click on the microbead and select **Stop Oscillating**.

7. Spinning disk confocal microscopy

1. Turn on the spinning-disk confocal microscope and accessory equipment, the integrated laser engines, and the acquisition cameras.
2. Launch the imaging software.
3. Set imaging channels for Hoechst staining of the nucleus and GFP for the cell plasma membrane.
   1. Activate the 405 nm and 488 nm excitation lasers lines.
   2. Add a multiband dichroic to reflect the excitation to the sample and that allows emitted light to pass to the cameras.
   3. Split the fluorescence emission with a 500 nm long pass edge dichroic mirror.

4. Use the DAPI/BFP (~445 nm) and GFP (~521 nm) emission filters in front of the two acquisition cameras, respectively. Refer to **Figure 2F,G**.
5. Set the exposure time to 100 ms for each channel.
6. Set laser emission to obtain a power of 5 mW at the sample plane. To measure the power, use a commercial power meter.

4. Set the imaging protocol. To avoid spectral bleedthrough from the Hoechst channel into the GFP channel, the two dyes need to be imaged sequentially.
   NOTE: If a hardware synchronization exists between the AODs of the optical trap and the camera acquisition, make sure that the trigger polarity is set up correctly. If in doubt, consult your facility manager or microscope manufacturer.

8. Performing the nucleus indentation experiments

NOTE: Always turn off the optical traps-both using software and closing the shutter on epifluorescence port 2-when lifting the force sensor module and changing the sample. If not, serious damage to optical elements and the experimenter could occur. Be careful with the lateral distance between lens holder and bottom dish edge when looking for cells to avoid bumping the lens into the stage/culture dish (**Figure 2**).

1. Place the sample in the microscope and follow step 5.3 of this protocol.
2. Using the rotating HWP (**Figure 2F**), set the trap power to 200 mW as a starting value if the stiffness of the nucleus or intracellular structure investigated is not known. Translate the OTs working area (using the microscope stage) to a place free of cells in order to compensate for the initial momentum baseline through step 6.5.

   NOTE: Depending on the stiffness of the subcellular structure, the trap power value should be adjusted to lower or higher values to obtain a similar indentation depth.
3. Using the microscope stage software controller, look for a cell with one or two beads through transmitted brightfield microscopy (**Figure 3A**).
4. Define a trap trajectory.
   1. Open the **Trajectory** dialog in the **Tools** submenu and choose **Displacement in the Trajectory Type** selector ring.
   2. In the numerical sheet, write the displacement and time of each subsequent trajectory step. Here are two examples.
   3. For a stress relaxation experiment, program trapezoidal loads, as shown in **Figure 3B**. In **Table S1**, two trapezoidal indentations were applied with a travel distance of 5 µm; velocity of 5 µm/s; waiting time before retraction: 10 s.
   4. For a repetitive indentation experiment at a constant velocity to obtain a triangular routine without dwell time on the nucleus, set the trajectory amplitude, e.g., 5 µm, and the time for the step, e.g., 2 s for a velocity of 2.5 µm/s. In **Table S2**, this is applied eight times at the same velocity.
      NOTE: These values need to be determined for each cell type and experiment, but the following parameters of a trapezoidal routine capture the most important dynamics in the experiment presented here. The waiting time should be sufficient for the nucleus to show its complete stress relaxation after indentation
5. Trapping a microsphere

1. Set the image plane slightly above the bead with the microscope stage software controller.
2. Activate traps using the OTs software and click on the bead in the camera AUX imaging window (calibrated following step 6.4). Successful confinement of the bead by the optical trap will strongly reduce the motion of the bead.
3. Click-and-drag the bead across the cytoplasm and place it at a distance of ~2 µm from the nuclear envelope (**Figure 3A**). Make sure that the trajectory is set so that the bead indentation is perpendicular to the nuclear membrane.

6. Optionally, if needed for position measurements of the bead relative to the trap, scan the trap across the bead to determine the trapping stiffness, k [pN/µm][54], thereby $\Delta x_{bead} = -F/k$ (see Discussion). The optical micromanipulation module used in this protocol has a built-in routine for this purpose.
   1. Open the **Particle Scan** dialog in the **Tools** submenu.
   2. Select the trap you want to scan and **High Frequency** as the **Scanning Method**. Select the direction (x or y) of the indentation trajectory for the bead scanning measurement.
   3. A window will appear with the measurement of the trapping stiffness. In the graph, drag the two cursors to select the linear trapping area corresponding to $F = -kx$. The linear fit to the selected data portion will be refreshed automatically.
      NOTE: Set the initial position of the bead far from the cell membrane (~5 µm), as light-momentum deflections at the medium-cell interface affect the appropriateness of force measurements. If the nucleus is located too close to the cell membrane, try to indent the nucleus from the opposite site. Discard the cell if not possible.
7. Start image acquisition by clicking on the acquisition button in the imaging software.
8. Start trap position and force measurement data saving by clicking on **Data | Save** in the real time force reading window (opened as in step. 6.6.1).
   NOTE: The optical trap is equipped with a trigger input which can be connected to the timing output of the camera. Thus, image and force data are hardware-synchronized and the electronic is able to map the trap cycles with the number of frames of the images during the acquisition.
9. Initiate the previously loaded trajectory by right-clicking on the bead and selecting **Start Trajectory**.
10. Wait until the trajectory is finished and the system stabilizes.
11. Stop trap force measurement data saving. A data saving dialog will pop up.
    NOTE: To optimize data storage, data can be decimated by selecting the decimating parameter in this dialog (10, 100, or 1000).
12. Stop image acquisition and plot the results in the postprocessing software of the user's choice.
13. If the microsphere is lost during the routine and the nucleus cannot be indented (**Figure S2**), discard the measurement and increase the power. Note that step 6.5 must be repeated. In our hands, at least 95% of the routines are successfully completed without losing the bead from the trap.

Representative Results

Microinjection of trapping beads:

Microspheres injected into the one-cell zebrafish embryo spread over the entire animal cap during morphogenesis. For a clearer visualization, we repeated the injection protocol with red fluorescent microbeads and took volumetric images with our confocal microscope at different developmental stages. In **Figure 4A-D**, injected beads are visualized in the cytoplasm of progenitor stem cells *in vivo* at 5 hfp. Later on, microspheres appeared spread over the whole embryo at 24 hpf (**Figure 4E**). Embryos at both stages developed normally and survival rates were comparable with control non-injected or mock-injected embryos (see **Figure S3**). This is consistent with other studies that report unperturbed survival of bead-injected zebrafish up to 5 days post fertilization[55].

Our spinning-disk confocal microscope is compatible with multi-channel fluorescence microcopy. In **Figure 5A**, we show isolated stem cells with one or two beads in the cytoplasm. Multiple fluorescent labels can be used to investigate different aspects of the cell (**Figure 5B**). Nuclear morphology can be tracked with a Hoechst dye or using a H2A::mCherry mRNA expression, while inner nuclear membrane can be analyzed with Lap2b-eGFP[12]. Dynamics of the actomyosin cortex, as well as intracellular calcium levels, can be observed with a My12.1::eGFP transgenic line[56] and Calbryte-520 incubation, respectively. The protocol that has been described here aims to compare cell nucleus mechanics of immobilized wildtype cells on adhesive substrates (later referred to as suspension) and in mechanical confinement. Isolated stem cells confined in microchambers of 10 µm height exhibited partial unfolding of the inner nuclear membrane (INM) and a subsequent increase in actomyosin contractility[12]. In **Figure 5C**, confined cells with one or two beads in the cytoplasm are shown. Successful confinement will be visible *via* flattened, expanded cells with a wider cross section of the nucleus. The nuclear membrane is further unfolded in confined cells and should appear smoothened out in comparison to cells in suspension (**Figure 5C**).

Force-time and force-deformation analysis

The analysis of the obtained results strongly depends on the investigated specimen and the question of interest and thus they cannot be generalized here. As an example, a common way to analyze indentation measurement is to extract a Young's modulus by fitting a modified Hertz model to the force-indentation data[57]. However, the assumption for such a treatment needs to be carefully assessed and might not always be properly justified (such as the investigated structure being isotropic, homogenous, with linear elasticity and indentations being smaller than the bead radius). We thus only consider model independent measurements here that allow the mechanical behavior of the investigated structure to be compared among different experimental scenarios.

As a starting point, measuring the slope of the force-displacement curve at a certain indentation depth provides a measure of a model independent structural stiffness[58] of the nucleus. This value can then be collected from multiple samples and compared between varying experimental settings and sample perturbations.

Indentation measurement

In the following lines, we focus on the mechanical response of the cell nucleus during cell deformation in confinement. Experiments in step 8 of this protocol typically lead to force peaks of up to 200 pN for indentation depths of approximately 2-3 µm. However, these values can be largely different, depending on the cell type and experimental conditions, with

softer nuclei leading to lower force for a given indentation. It is thereby needed to accurately measure the nuclear deformation, together with force, for an accurate mechanical characterization of the cell nucleus. In this section, we will obtain the cell nuclear stiffness from representative force indentation measurements.

In **Figure 6**, we show the deformations of the distal and proximal sides of a nucleus in a suspended and confined cell. A rich mechanical behavior can be observed. In a typical suspended cell on an adhesive substrate, the nucleus was strongly indented by the bead, but also slightly displaced upon repetitive pushing events. We measured the bead indentation onto the nucleus by analyzing the kymographs obtained from fluorescence imaging of Hoechst-stained cell nuclei. Kymographs were easily computed using Fiji's Multi Kymograph plugin along the indentation direction (**Figure 6A,B**) and imported into Matlab (Version 2021, Mathworks) for further processing. A step function was fitted to the raw intensity profile with the aim to track the delimiting edges of the nucleus along the trajectory of the indentation routine. As can be seen, it bears accurate information on the nuclear change in shape (**Figure 6** and **Figure S2**). We used the following double-sigmoid curve as an analytical version of a step function:

$$I(x) = (A - B)\left(\frac{1}{1 + exp\left(-\frac{x - x_1}{\epsilon_0}\right)} - \frac{1}{1 + exp\left(-\frac{x - x_2}{\epsilon_0}\right)}\right) + B$$

(Equation 1)

Here, x_1 and x_2 denote the distal and proximal edges of the nucleus, while A and B are the maximum and background gray values of the blue channel (Hoechst dye) of the image (**Figure 6B**). The edge width has been considered (e_0 = 0.25 mm). While the indented, proximal nucleus edge (x_2) followed the trajectory applied by the optical trap routine after the microsphere-nucleus contact, the opposite, distal edge (x_1) displays relaxation dynamics as expected for a viscoelastic material such as the cytoplasm (**Figure 6D**). In contrast, nuclei in cells confined in 10 µm high microchambers do not exhibit such translocation behavior of the nucleus upon indentation within the cell (**Figure 6B,D**). Also shown in **Figure 6D**, the rear edges of the nuclei remains unaltered by the bead pushing from the proximal side, most likely due to stronger forces arising from cell contractility and friction acting against the indentation force. In order to get the correct deformation depth, the displacement *x1* was subtracted from the indented measure x2: $\Delta x = x_2 - x_1$ (see also **Figure 6D**).

Force data analysis

The force causing nuclear deformation was measured from the change in light momentum originated at the optically-trapped microbead (**Figure 7A**). The force upon applying trapezoidal trajectories (step 8.4.3, **Figure 7B**) initially increased linearly until the trap stopped moving, but then relaxed to a steady state value. This behavior indicated a viscoelastic material exhibiting loss and storage moduli. Right after the indentation event, the force reached a peak value, F_0, followed by a stress relaxation (**Figure 7C**):

$$F(t) = F_0 + (F_p - F_0)\, f(t)$$

(Equation 2)

where F_0 is the stored force for the elastic component and $f(t)$ is a dimension-less relaxation function. We have analyzed this behavior in three ways:

1. Considering a standard linear solid with an exponential stress relaxation, i.e., $f(t) = e^{-t/\tau}$, schematically represented in **Figure 7C** inset.

2. Using a general, double-exponential decay:

$F(t) = A + B_1 e^{-t/\tau 1} + B_2 e^{-t/\tau 2}$.

3. Using a power law followed by an exponential decay[59]: $f(t) = t^{-p} e^{-t/\tau}$, fitted in **Figure 7C**.

While the fit for model 1 can be carried out straightforwardly, we recommend to estimate the initial guesses for (τ_1, τ_2) and (p, τ) for models 2 and 3, respectively. This can be performed, respectively, by fitting lines onto the data in logarithmic-versus-linear (**Figure 7D**, left) and logarithmic-versus-logarithmic (**Figure 7D**, right) scales. **Table S3** summarizes the results for the example analyzed in **Figure 7**. In the following section, we will consider the combination of a power law and an exponential law for the characterization of the cell nucleus mechanics.

Force displacement relation

Likewise, the described experimental set-up can be used to obtain the force-displacement relation of multiple indentation events. By performing triangular routines (step 8.4.4, **Figure 8A**), it is possible to relate the force to the deformation and plot a force-indentation curve. An exemplary outcome is shown in **Figure 8B**, in which a flat baseline smoothly changed slope once the bead got into contact with the nucleus. Identifying the true contact point in the noisy data is a challenge, and care has to be taken to see whether the contact region is fit to elastic models[60]. In this particular experiment, it could also be seen that the subsequent indentations result in curves with deeper contact points, indicative for too slow nuclear shape recovery after bead retraction and a change in the hysteretic cycle defined by the nucleus viscoelastic material properties (**Figure 8C**). Thus, the researcher should be aware if this happens and incorporate this into the analytical pipeline, or restrict the number of subsequent measurements such that this effect does not modify the measurement.

Nucleus mechanics in cells in suspension and under 10 µm confinement

The aforementioned approach was used to analyze the dynamics of nucleus stress relaxation in suspended cells on adhesive substrates and confined cells. Our results show that the confinement results in an expansion of the projected area (**Figure 9A**), but insignificant change in nuclear stiffness (**Figure 9B**). We measured similar relaxation with τ = 6.08 ± 1.1 s (unconfined) and τ = 4.00 ± 0.6 s (confinement), which indicates fast viscoelastic dissipation, followed by a stored force value that corresponds to the elastic modulus of the nucleus. In order to account for experimental variations, which may be produced by different initial conditions in the indentation routines, measured stored forces were normalized to the indentation depth, as $F_0/\Delta x$. This parameter accounts for the nucleus stiffness and describes the force, or the stress, necessary for a certain indentation. We obtained similar stiffness under confinement and in unconfined cells: $F_0/\Delta x$ = 20.1 ± 12.6 pN/µm and $F_0/\Delta x$ = 24.6 ± 13.6 pN/µm (mean ± standard deviation), respectively.

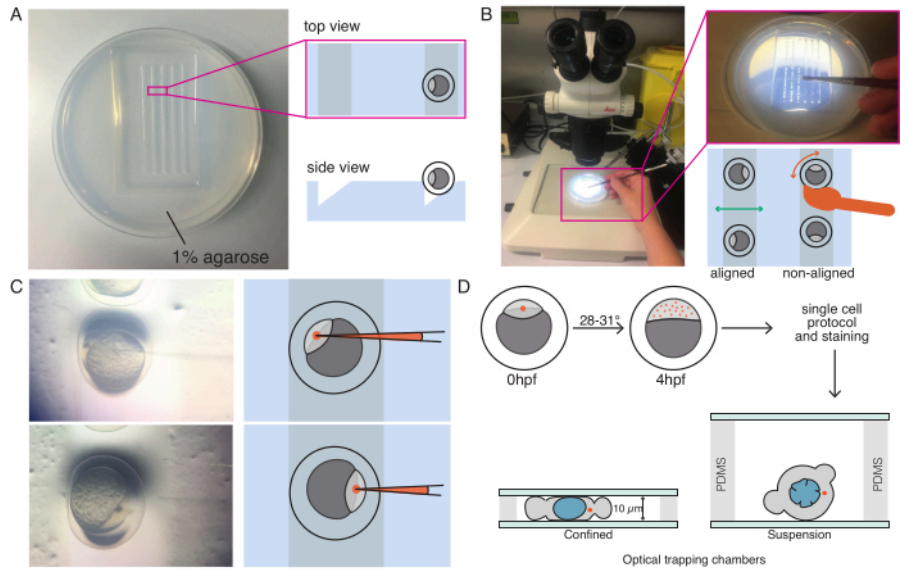

Figure 1: Microinjection of zebrafish embryos at one-cell (zygote) stage. (**A**) Injection plate: a triangular-shape injection plate is used for the injection. The plate is made of 1% ultrapure agarose in E3 (Egg's medium). Top and side views are shown on the right. (**B**) Embryo positioning: gently orient the embryos using a brush and orient such that the one-cell is clearly visible and easily accessible with the needle. We suggest to orient the embryos with the cell located in the opposite side of the needle, as shown in the sketch. (**C**) Injection procedure into the one-cell stage embryo: pierce the chorion surrounding the embryo and the single cell with the needle. Be sure that the tip of the needle is inside the cell and release the pressure to inject. (**D**) Incubate the embryos at 28-31 °C until they develop up to the blastula (sphere) stage (4 hpf). Perform the cell isolation protocol and cell staining (step 2) and prepare the optical trapping chamber with isolated cells in suspension and/or confinement combined with the corresponding substrate surface coating (step 3). Please click here to view a larger version of this figure.

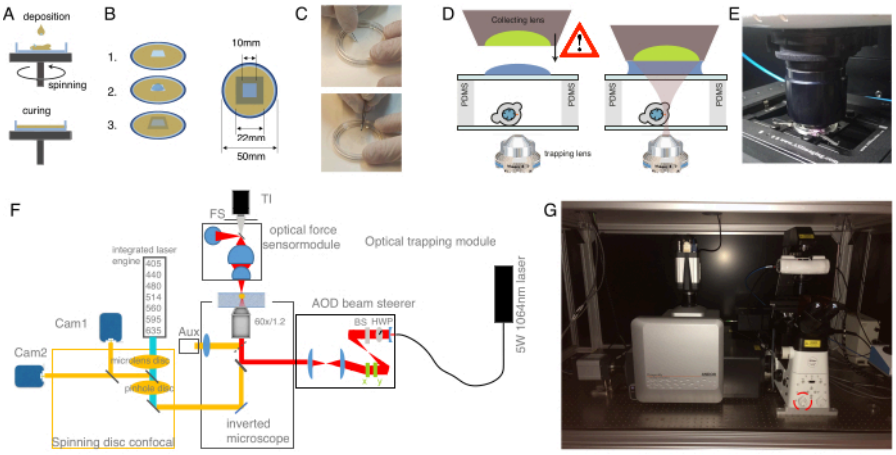

Figure 2: Preparation of the optical tweezer apparatus. (**A**) Spin-coating layers of PDMS with a defined height onto glass bottom dishes. The PDMS drop will spread out evenly due to the centrifugal force. (**B**) Preparation of the sample chamber out of the PDMS layer. 1: cut a square with a scalpel, 2: coat the inner well with concanavalin A (ConA), wash and seed cells; 3: cover with a glass slide or cover slip to seal the well. (**C**) Picture of the square cutting with a scalpel and removing the PDMS well with forceps. (**D**) Mounting the collecting lens of the optical force sensor over the trapping chamber. A drop of immersion oil serves as an immersion medium between the collecting lens and the upper glass cover. Schematic not to scale. Be cautious while lowering the collecting lens to not touch the glass cover of the sample dish. (**E**) Picture of the force detection unit in contact with the sample. (**F**) Schematic of the experimental set-up. The optical micromanipulation module uses a continuous wave laser beam (5W, λ = 1064 nm) with power control through a half-wave plate (HWP) and a polarizing beam splitter (BS). After being modulated with a pair of AODs, it is coupled to the upper epifluorescence port of an inverted microscope. The laser beam is then reflected by a 950 nm short-pass dichroic mirror (IR-DM), allowing for transmittance of fluorescence excitation and emission. The trapping laser is guided into the rear, epifluorescence port of the microscope (upper turret). The OTs are created at the focal plane of a water-immersion objective lens (60x, NA = 1.2). The optical force sensor is subjected by the microscope turret and captures the laser light emerging from the OTs with a high-NA, oil-immersion lens. At the same time, the force sensor enables bright-field illumination. The spinning-disk confocal unit is coupled to the left port. It is equipped with two integrated laser engines (ILE) that control seven fluorescence excitation lasers and two back-illuminated sCMOS cameras, enabling for dual fluorophore imaging in parallel Abb: TI, Transilluminator; FS, field stop; AOD, acustooptical deflector; HWP, half wave plate; CAM, camera (**G**) Photograph of the optical trapping equipment. Red circle indicates the Bertrand lens, that can be switched into the optical path manually. Please click here to view a larger version of this figure.

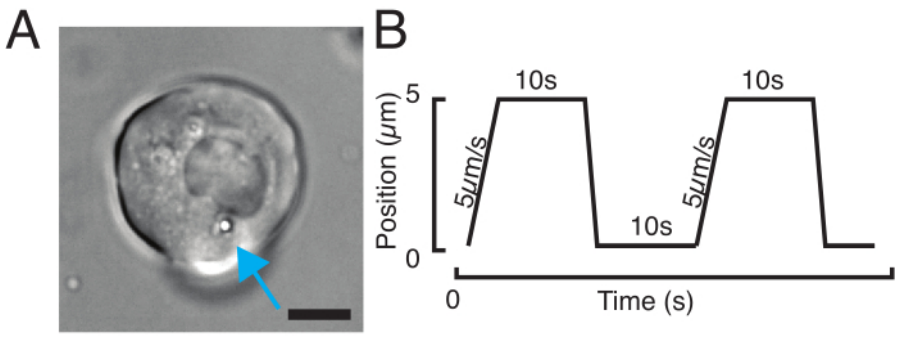

Figure 3: Choosing the right samples and parameters. (**A**) Representative image of an isolated zebrafish progenitor stem cell with a single microsphere positioned close enough to the nucleus to perform the indentation experiment. Scale bar = 10 µm. (**B**) Exemplary trap trajectory; indentation depth 5 µm; indentation speed = 5 µm/s; relaxation time 10 s. Please click here to view a larger version of this figure.

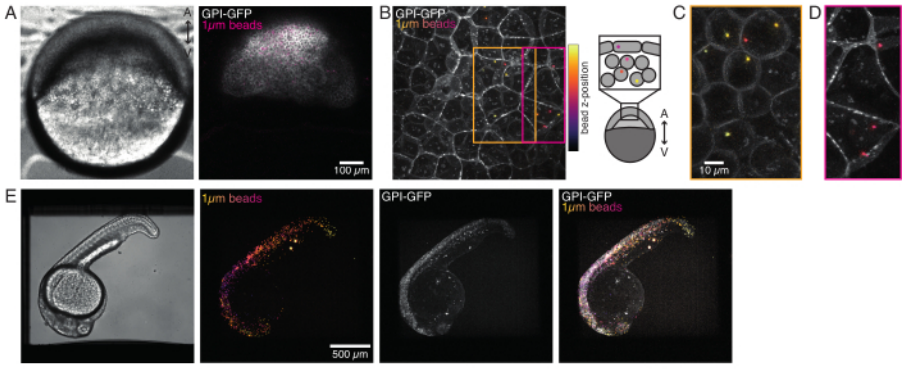

Figure 4: Microbead localization inside zebrafish embryos during development. 0.5 nL of 1 µm red fluorescent beads are injected together with GPI-GFP mRNA (100 pg/embryo, plasma membrane) in WT embryos to visualize bead localizations. (**A-D**) Distribution of microsphere 5 h post injection inside an embryo mounted in 0.75% agarose. (**A**) Brightfield and fluorescence image. The beads are homogenously dispersed across the embryo tissue as seen in a confocal micrograph. (**B**) Maximum projection of confocal fluorescence z-stack. The beads are color-coded from purple to yellow according to their z-position in the image stack. Purple/magenta corresponds to the most outer beads/cells (EVL; epithelial enveloping layer; or progenitor stem cells located close to the EVL surface), yellow corresponds to inner beads (progenitor deep cells), as shown in the sketch on the right. (**C**) Cut and maximum projection of a sub-stack of (**B**) corresponding to the region in the orange box: a large fraction of deep cells contain 1-2 beads. (**D**) Cut and maximum projection of a sub-stack of (**B**) corresponding to magenta box: some EVL cells contain 1-2 beads. (**E**) Brightfield image and maximum projection of a z-stack of a 24 hpf embryo mounted in 0.75% agarose and anesthetized with tricaine. Embryos were pre-incubated with tricaine for 15 min. From left to right: microspheres (1 µm diameter), GPI-GFP and image overlap. The beads distributed across the entire body of the embryo. Scalebar dimension indicated in each panel. Please click here to view a larger version of this figure.

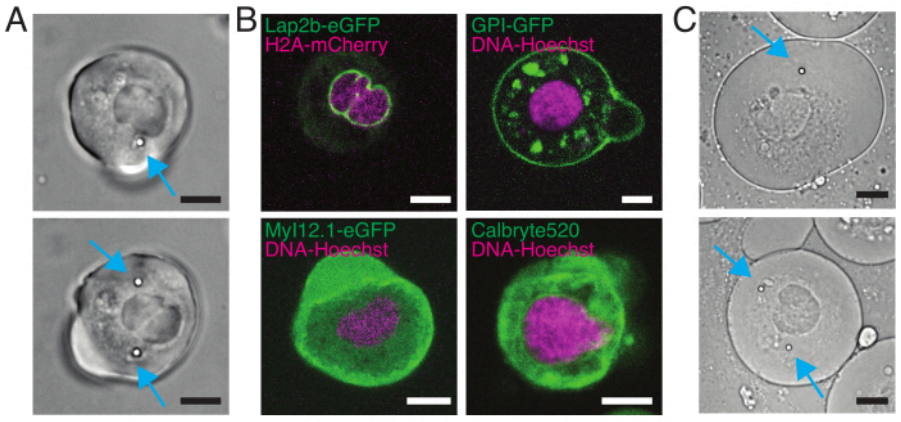

Figure 5: Isolated zebrafish progenitor stem cells with different labeling. (**A**) Transmission light microscopy image of suspension cells with 1 (top) or 2 (bottom) injected beads. Cyan arrows point at beads. (**B**) Fluorescent confocal images of suspension cells with different stainings. Top-left: Lap2b-eGFP (inner nuclear membrane, 80 pg/embryo) and H2A-mCherry. Top-right: GPI-GFP (plasma membrane, 100 pg/embryo) and DNA-Hoechst (stained as described in section 2). Bottom-left: Myl12.1-eGFP (transgenic line) and DNA-Hoechst. Bottom-right: Calbryte488 and DNA-Hoechst (stained as described in section 2). (**C**) Transmission light microscopy image of confined cells with 1 (top) or 2 (bottom) injected beads. Cyan arrows point at beads. Scale bars = 10 µm. Please click here to view a larger version of this figure.

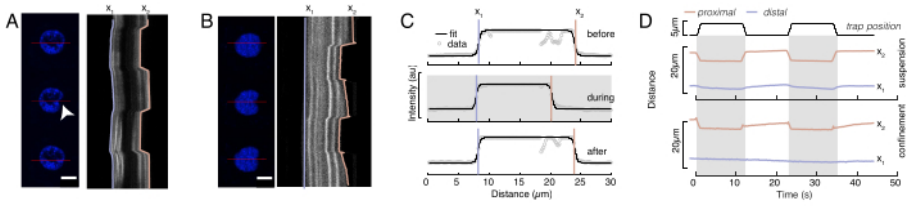

Figure 6: Estimating nuclear deformation from spinning disc movies. (**A,B**) Time-lapse of an indentation experiment of the nucleus in (**A**) a suspended cell and (**B**) a confined cell. Scale bar 10 μm. Representative snapshots of a Hoechst-labeled nuclei are shown 5 s before, during, and 5 s after indentation with an optically-trapped microsphere (white arrowhead). Kymographs along the indentation segment (red line, right panel). x_1 and x_2 are the distal and proximal (close to the bead) boundaries of the nucleus during the indentation experiment extracted from the fit of the intensity profile to Equation 1. (**C**) Intensity profiles along the indentation segment for three different frames (before, during and after indentation) and fitted to Equation 1 to assess the distal, x_1, and proximal, x_2, positions of the nucleus edges. (**D**) Representative trajectories of $x_1(t)$ in blue and $x_2(t)$ in amber during an indentation experiment of suspended and confined cells (10 μm). Shaded areas indicate the indentation, the distance between x_1 and x_2 indicates the nucleus diameter. Please click here to view a larger version of this figure.

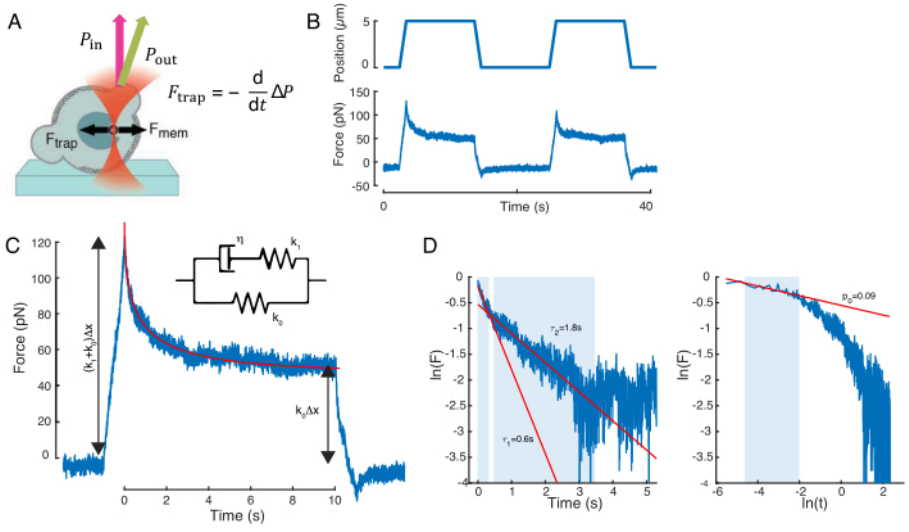

Figure 7: Force signal processing. (**A**) Schematic of an optically-trapped microsphere deforming the cell nucleus upon indentation. Nuclear membrane and optical forces are indicated by the black arrows. The change in beam momentum is indicated by the green arrow P_{out}. (**B**) Trap trajectory (top) and force (bottom) experienced by the optically-trapped microsphere during a repeated nuclear indentation experiment. (**C**) Force relaxation decay after the force peak at the maximal indentation depth. Inset shows a schematic of standard linear solid whose dynamics approximate the phenomenological observations here. (**D**) Left: logarithm of the normalized force versus time. The shadowed areas indicate the data portion used to fit the double exponential decay (red lines). Right: logarithm of the normalized force versus the logarithm of time. The shadowed area indicates the data portion used to fit the power law. Please click here to view a larger version of this figure.

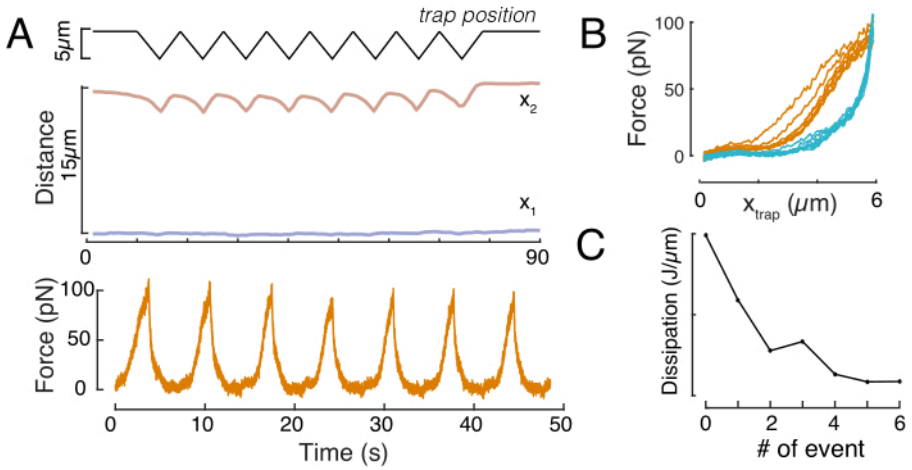

Figure 8: Force indentation routine with triangular trap displacements. (**A**) Representative trajectory of $x_1(t)$ in blue and $x_2(t)$ in amber during a triangular indentation experiment taken on a cell in 10 µm confinement height. Top: Trap position. Middle: Nucleus shape analysis. The distance between x_1 and x_2 indicates the nucleus diameter. Bottom: Force signal. (**B**) Force vs trap position for eight consecutive indentations. (**C**) Evolution of the dissipation, derived from the hysteresis between the approach and withdrawal part of the f-d curve, of the nucleus for each subsequent indentation event. Please click here to view a larger version of this figure.

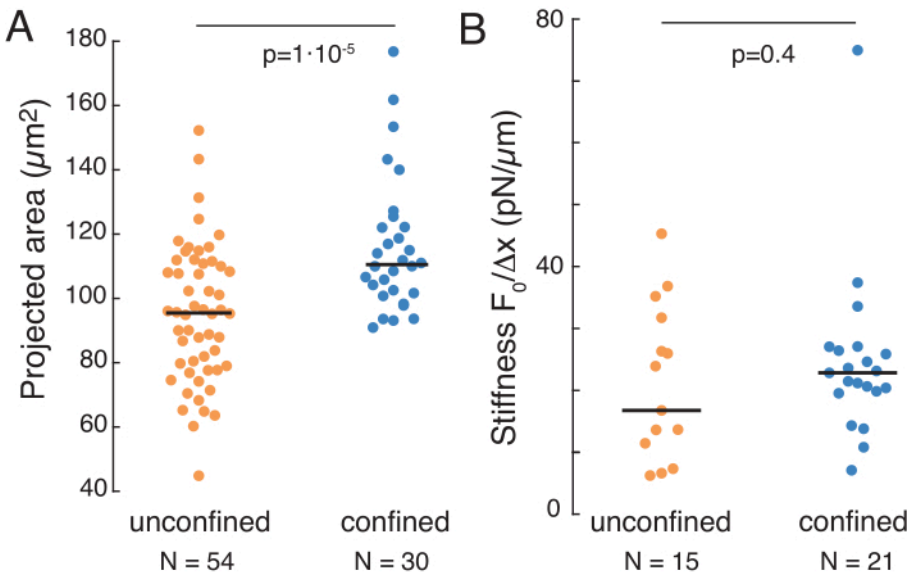

Figure 9. Nuclear properties of cells in suspension (adhesive surface) and confinement from trapezoidal routines. (**A**) Projected area of the nucleus from cells in suspension and under 10 μm confinement. Black bar represents the median. (**B**) Nuclear stiffness of cells in suspension and under confinement. Black bar represents the median. P-values derived from Kruskal-Wallis test using MatLab. Please click here to view a larger version of this figure.

Supplemental Table 1: Trapezoidal trajectory defined by the optical tweezers software. First (second) row is the x (y) distance that the trap will be linearly displaced. On the third row, the duration of a given step is set in seconds. This trajectory is composed of seven points and corresponds to the trapezoid loaded two times against the nucleus in **Figure 7B**. Please click here to download this Table.

Supplemental Table 2: Triangular trajectory defined by the optical tweezers software. Analogous to Table 2, this trajectory is composed of 16 points, corresponding to eight indentation events at a depth of 5 μm and a velocity of 2.5 μm/s. Please click here to download this Table.

Supplemental Table 3: Fitting parameters for the data in Figure 7. IG: initial guess. Please click here to download this Table.

Supplemental Figure S1: Optical force sensor alignment and momentum baseline compensation. (**A**) Field stop imaged at the auxiliary camera (AUX, **Figure 2**) through the Bertrand lens. An air bubble appears visible in the immersion oil, which is not visible through the eyepiece. (**B**) Clean optical path. For accurate alignment, open the field stop and make it coincide with the NA = 1.2 light cone. (**C**) Image of the sample plane. The red square indicates the OT working area. Scale bar: 20 μm. (**D**) Trap power measured across the FOV, along white double arrows indicated in C. In red, trap power variation when no correction is applied. In blue, trap power corrected over the entire field of view. (**E**) X-component of

the momentum baseline along the same range. In red, non-corrected trace. In blue, trace corrected for trap power. In green, trace corrected for momentum baseline using Global Offset Compensation in the manufacturer's software. (**F**) Same as in E, for the Y-component. Note that under normal operation, the shaded components are used for mechanics and force measurements, e.g., x force component during movement along the x coordinate and the y force component during movement along the y-axis. After all the corrections are implemented, an RMSD noise of <0.5 pN is obtained. Please click here to download this File.

Supplemental Figure S2: A failed routine due to weak traps. (**A)** Kymograph showing a nucleus indentation from a failed routine. Only short, transient deformations are visible due to an escape of the bead from the trap. Importantly, the trapping laser still moves without bead to complete the predefined trajectory (green dotted line). Scale bar = 10 µm. (**B**) Top: Trap position versus time. Middle: Edge tracking result of the indented proximal and distal nucleus edge. Note that the distal edge is not moving without the indentation as commonly observed for completed routines on isolated cells on adhesive substrates. Bottom: Force versus time showing the loss of the microsphere indicated by a reduction in thermal noise and a sudden drop to zero force. Please click here to download this File.

Supplemental Figure S3: Survival of injected embryos. Embryos injected with 1 µm beads and 100 pg/embryo of mRNA at concentrations outlined in the protocol were compared to uninjected embryos and show no significant differences 24 h post fertilization. Mean and standard deviation of three independent experiments with N > 21 embryos per condition for each experiment. Please click here to download this File.

Discussion

In this protocol, we describe a unique method to interrogate the mechanical properties of the cell nucleus inside the living cells. Different to other force spectroscopy techniques, non-invasive optical trapping allowed us to decouple the contribution of the cell membrane and cytoskeleton from the cell nuclear stiffness. Importantly, optical micromanipulation is compatible with multimodal microscopy, which will allow the experimenter to study different processes involved in cell nuclear mechanobiology. As a representative result, we used DNA-Hoechst staining to measure the nucleus deformation upon indentation performed by forces of the order of several hundreds of picoNewton.

Potential applications of our method beyond the examples outlined in this protocol

The possibility to extract quantitative mechanical information from measurements inside living cells without external perturbations enable a plethora of unprecedented opportunities that are just beginning to be explored. Thus, the presented protocol of our optical micromanipulation platform can be extended to more complex experiments with great versatility. Acousto-optic deflectors (AOD) can generate multiple optical traps for synchronous force measurements across different cell locations, as well as can be used for active microrheology in a wide frequency range[51,61]. As has been mentioned, the force response upon indentation can overcome the maximum trapping force, leading to an escape of the bead from the optical trap. In this case, a force feedback can be configured with the AOD in order to clamp the optical force. All in all, multiple microrheological approaches, such as the stress relaxation described in this protocol, but also active microrheology or creep compliance, can be experimentally obtained with this platform and thoroughly analyzed by novel software

packages[61,62,63,64,65]. Furthermore, the application of forces is not limited to the nucleus but could in principle be carried out to measure diverse intracellular structures and in complex tissues as demonstrated for trapping flowing red blood cells inside intact blood vessels[66,67] or trapping and deforming chloroplasts and mitochondria[68]. Light-momentum calibration is independent of the shape and size of the trapped object, hence enabling direct force measurements on any force probe with arbitrary shape[38,39]. The use of injected microspheres allowed us to apply high forces onto the nucleus with relatively low laser power as compared to direct manipulation of cellular structures[69,70,71]. However, given a high enough refractive index difference, no externally applied force probe is necessary and intracellular organelles can be manipulated directly without injected beads (unpublished observations and reference[70]).

Potential modifications of our method to extend the applications

Different sizes of microbeads can be injected depending on the experiment, but the relative controls must be done. For example, to study cells at later stages smaller beads can be injected. This will reduce the maximum force that can be exerted by the optical trap (such as shown in reference[55]). Bigger beads can be injected to exert higher forces, but these might affect embryo development depending on their size or stage of interest. In experiments where microbead injection is not an option, various organelles displaying refractive indices differences compared to that of the cytoplasm can still be optically manipulated, giving rise to optical forces measurable from light momentum changes[42]. As mentioned above, these methods have been employed by Bambardekar et al. to deform cell-cell junctions in the Drosophila embryo[70]. Likewise, the cell's nucleus has a lower refractive index than the surrounding medium[44], which allows for bead-free indentation (unpublished observations and reference[72]) even though with a lower trapping strength. Thus, the nucleus cannot be trapped easily and escapes the trap.

The spin-coated PDMS spacer is fabricated *via* a convenient and fast method but might be out of reach for labs without access to a micro-/nanofabrication facility or engineering labs. Thus, the spacer can be easily assembled from lab tape or parafilm (step 4). The protocol can also be adapted by manufacturing microfluidic channels that automate the delivery of single cells into predefined measurement wells or into a chamber with a defined height to estimate the confinement effect within the same specimen. However, such microfluidic devices must be designed so that they fit the space between the microscope objective and the collecting lens of the optical force sensor, of around 2 mm (see step 3). Note that the optical force sensor must be positioned at the appropriate height so that no optical aberrations from defocusing affect the photon momentum measurement.

Other modifications could include the change of biological reporters. We found that Hoechst fluorescence spectrally bleeds into the GFP channel and we thus favor the combination with mCherry-tagged histone as a nuclear marker for simultaneous measurement in two fluorescent channels. Alternatively, nuclear deformation can easily be tracked with a label targeted to the inner nuclear membrane such as Lap2b-GFP (**Figure 2**).

Indentation onto the cell nucleus was of the order of 2-3 microns, which we could accurately measure by image analysis of diffraction-limited spinning-disk confocal microscopy. For the case of stiffer nuclei or smaller forces, indentation will be barely measurable using this approach. However, the absolute force-calibrated optical tweezers can be also calibrated for position measurements of the

trapped bead *in situ* using BFP interferometry with nanometer accuracy[51]. Using this approach, the voltage signal and the optical force sensor can be translated into the position of the trapped probe through parameter β [nm/V], while the invariant parameter α [pN/V] yields force values through the aforementioned light-momentum calibration[41] (see below for details).

Troubleshooting

We found that the following challenges could occur during the experiment:

No stable trap is formed and the microsphere escapes easily

Any dirt on the microscope objective or a misaligned correction collar could lead to a failure of a stable trap. If an immediate solution is not found, measure the point-spread function of the objective lens. If the specimen of interest is deep inside an optically dense tissue, the laser focus might experience severe optical aberrations leading to unstable trapping (this effect is usually negligible in isolated cells but becomes more evident in thicker tissues). For high stiffness, the restoring force of the nucleus could exceed the escape force of the trap, such that the microsphere is lost and the indentation routine fails. Initially, the nuclear membrane edge proximal to the optical trap gets hardly indented (**Figure S2A**). When this occurs, the trapping laser is no longer affected by force and Brownian motion, which leads to a force drop to zero and a decrease of the signal noise (**Figure S2B**). In case this happens, laser power can be increased to have a stronger trap, the amplitude of the trapezoidal trajectory pushing the bead into the nucleus can be reduced, or the initial position of the trapped microbead can be set further off the nucleus.

The cell is moving during the stimulation

If cells are not sufficiently attached, the optical gradient trap will move the cells while performing the intracellular indentation routine, such that the forces and underlying mechanics of the nucleus are artefactual. To prevent displacement of the entire cell, we recommend increasing the concentration of cell adhesion molecules on the surface, e.g., ConA.

Initial momentum compensation

If an initial momentum compensation routine is not available in the OTs platform (step 6.5), an artificial, force-independent baseline signal needs to be corrected for. This is visible as a slope on the force curve even with no bead trapped (**Figure S1E**). To do the correction, the same trajectory needs to be performed without a bead, outside of the cell at exactly the same position. For this, move the cell away from the trap using the stage control. As a reference, the force offset changes 5 pN across the FOV at 200 mW in our system; thus, it becomes negligible for short trajectories. Alternatively, a piezo scan stage can be used to move the cells on the sample, leaving the laser position constant.

Critical steps of the presented protocol

Microspheres should be injected at the right, 1-cell stage to ensure maximal distribution over the embryo. Beads should not be fluorescent so that no light leaks into the fluorescent channels used for imaging. For example, even typical red-fluorescent beads are clearly visible in the blue channel used for imaging the cell nucleus after Hoechst staining due to their brightness (excitation: 405 nm; emission: 445 nm). Stable attachment of the cell to the substrate is critical to prevent lateral displacement during the indentation routine. If the cell moves during the routine, forces are underestimated. Should this happen frequently, optimize the attachment protocol. For tissue culture cells, other

cell adhesion proteins, such as fibronectin, collagen, or poly-L-lysine lead to satisfactory attachment (unpublished observations). During the confinement, cells are subjected to a sudden and severe mechanical stress. This can cause damage to the cells and frequently the experimenter will encounter bursted cells if the procedure is not carried out carefully. Also, if the confinement height is too small, all the cells will suffer from nuclear envelop breakage or irreversible damage. To mitigate these, lower the upper coverslip more slowly and/or increase the spacing between the coverslip.

Limitations of the technique and suggestions to overcome them

A clear limitation of the technique is the penetration of the laser light into deep sections of the tissue, which leads to aberrations and unstable trapping. Thus, a lower limit of penetration depth depends on the clarity of the sample, the aberration correction that can be employed[73] and the applied laser power. It should be taken into account that a higher laser power leads to thermal excitation of the sample in the vicinity of the microsphere. However, heating of the sample originated by the 1064 nm wavelength laser spot is minimized to avoid plausible heat-related stress onto our biological samples[74].

Another limitation is the maximum force that can be measured. Even though direct light-momentum detection enables force measurements far beyond the linear response regime of the optical trap[40,41], the maximum applied force is in the order of a few hundred picoNewtons. This is limited by laser power and the consequential damage threshold of soft biological material and the refractive index differences, which are normally not larger than 0.1 or 0.3[44]. Several methods have been proposed to increase the force detection limit, e.g., using structured light[75], anti-reflective coated microspheres[76], high-refractive index particles[77] or highly doped quantum dots[78].

OTs can be used for nanometer-scale position measurements through BFP interferometry, such that the position of the bead within the trap is $\Delta x = \beta S_X$, where S_X is the voltage signal of the sensor, and β [µm/V] can be calibrated on-the-fly following different protocols[35,54]. For an optical force sensor, it can be proved that the voltage-to-force invariant conversion factor α [pN/V] directly relates to β and the trap stiffness, k [pN/µm], through $\alpha = k\beta$ [37]) In experiments with bead displacements that are too small to be detected from optical imaging, this strategy can be used to complement force measurements with small position detection. An example is the application of the experimental routines presented here onto very stiff nuclei, for which forces at reasonable laser powers (200-500 mW) are not sufficient to induce indentation values large enough. In that case, the bead needs to be brought in contact with the nucleus and the trapping stiffness must be calibrated prior to the measurement (step 8.6). The indentation d of the nucleus as a function of force can be indirectly determined as:

$$d = x_{trap} - F/k$$

where x_{trap} is the trap position. Different to the invariant light-momentum factor α [pN/V], factor β [µm/V] needs to be calibrated prior to each experiment since it depends on many local variables determining the trapping dynamics, such as the particle size, optical trap spot size, and relative refractive indices.

Disclosures

The authors have nothing to disclose.

Acknowledgments

MK acknowledges financial support from the Spanish Ministry of Economy and Competitiveness through the Plan Nacional (PGC2018-097882-A-I00), FEDER (EQC2018-005048-P), Severo Ochoa program for Centres of Excellence in R&D (CEX2019-000910-S; RYC-2016-21062), from Fundació Privada Cellex, Fundació Mir-Puig, and from Generalitat de Catalunya through the CERCA and Research program (2017 SGR 1012), in addition to funding through ERC (MechanoSystems) and HFSP (CDA00023/2018). V.R. acknowledges support from the Spanish Ministry of Science and Innovation to the EMBL partnership, the Centro de Excelencia Severo Ochoa, MINECO's Plan Nacional (BFU2017-86296-P, PID2020-117011GB-I00) and Generalitat de Catalunya (CERCA). V.V. acknowledges support from the ICFOstepstone PhD Programme funded by the European Union's Horizon 2020 research and innovation program under Marie Skłodowska-Curie grant agreement 665884. We thank Arnau Farré for critical reading of the manuscript; Maria Marsal for the help with the imaging and mounting of the 24 hpf embryo and; Senda Jiménez-Delgado for support with zebrafish micronjections.

References

1. Chan, C. J., Heisenberg, C. P., Hiiragi, T. Coordination of Morphogenesis and Cell-Fate Specification in Development. *Current Biology.* **27** (18), R1024-R1035 (2017).
2. Heller, E., Fuchs, E. Tissue patterning and cellular mechanics. *Journal of Cell Biology.* **211** (2), 219-231 (2015).
3. Heisenberg, C. P., Bellaïche, Y. Forces in tissue morphogenesis and patterning. *Cell.* **153** (5), 948-962 (2013).
4. Petridou, N. I., Spiró, Z., Heisenberg, C. P. Multiscale force sensing in development. *Nature Cell Biology.* **19** (6), 581-588 (2017).
5. Krieg, M. et al. Tensile forces govern germ-layer organization in zebrafish. *Nature Cell Biology.* **10** (4), 429-436 (2008).
6. Ruprecht, V. et al. Cortical contractility triggers a stochastic switch to fast amoeboid cell motility. *Cell.* **160** (4), 673-685 (2015).
7. Shellard, A., Mayor, R. Supracellular migration - Beyond collective cell migration. *Journal of Cell Science.* **132** (8) (2019).
8. Mongera, A. et al. A fluid-to-solid jamming transition underlies vertebrate body axis elongation. *Nature.* **561** (7723), 401-405 (2018).
9. Atia, L. et al. Geometric constraints during epithelial jamming. *Nature Physics.* **14** (6), 613-620 (2018).
10. Turlier, H., Maître, J.-L. Mechanics of tissue compaction. *Seminars in Cell & Developmental Biology.* **47 - 48**, 110-117 (2015).
11. Ladoux, B., Mège, R. M. Mechanobiology of collective cell behaviours. *Nature Reviews Molecular Cell Biology.* **18** (12), 743-757 (2017).
12. Venturini, V. et al. The nucleus measures shape changes for cellular proprioception to control dynamic cell behavior. *Science.* **370** (6514) (2020).
13. Charras, G., Sahai, E. Physical influences of the extracellular environment on cell migration. *Nature Reviews Molecular Cell Biology.* **15** (12), 813-824 (2014).
14. Kirby, T. J., Lammerding, J. Emerging views of the nucleus as a cellular mechanosensor. *Nature Cell Biology.* **20** (4), 373-381 (2018).

15. Lee, H. P. et al. The nuclear piston activates mechanosensitive ion channels to generate cell migration paths in confining microenvironments. *Science Advances.* **7** (2) (2021).

16. Friedl, P., Wolf, K., Lammerding, J. Nuclear mechanics during cell migration. *Current Opinion in Cell Biology.* **23** (1), 55-64 (2011).

17. Versaevel, M., Riaz, M., Grevesse, T., Gabriele, S. Cell confinement: Putting the squeeze on the nucleus. *Soft Matter.* **9** (29), 6665-6676 (2013).

18. Zuela-Sopilniak, N. et al. Measuring nucleus mechanics within a living multicellular organism: Physical decoupling and attenuated recovery rate are physiological protective mechanisms of the cell nucleus under high mechanical load. *Molecular Biology of the Cell.* **31** (17), 1943-1950 (2020).

19. Kim, D. H., Wirtz, D. Cytoskeletal tension induces the polarized architecture of the nucleus. *Biomaterials.* **48**, 161-172 (2015).

20. Lomakin, A. J. et al. The nucleus acts as a ruler tailoring cell responses to spatial constraints. *Science.* **370** (6514) (2020).

21. Hampoelz, B. et al. Microtubule-induced nuclear envelope fluctuations control chromatin dynamics in Drosophila embryos. *Development.* **138** (16), 3377-3386 (2011).

22. Heo, S. J. et al. Differentiation alters stem cell nuclear architecture, mechanics, and mechano-sensitivity. *eLife.* **5**, 1-21 (2016).

23. Cosgrove, B. D. et al. Nuclear envelope wrinkling predicts mesenchymal progenitor cell mechano-response in 2D and 3D microenvironments. *Biomaterials.* **270**, 120662 (2021).

24. Liu, H. et al. In situ mechanical characterization of the cell nucleus by atomic force microscopy. *ACS Nano.* **8** (4), 3821-3828 (2014).

25. Hobson, C. M. et al. Correlating nuclear morphology and external force with combined atomic force microscopy and light sheet imaging separates roles of chromatin and lamin A/C in nuclear mechanics. *Molecular Biology of the Cell.* **31** (16), 1788-1801 (2020).

26. Pajerowski, J. D., Dahl, K. N., Zhong, F. L., Sammak, P. J., Discher, D. E. Physical plasticity of the nucleus in stem cell differentiation. *Proceedings of the National Academy of Sciences of the United States of America.* **104** (40), 15619-15624 (2007).

27. Rowat, A. C., Lammerding, J., Ipsen, J. H. Mechanical properties of the cell nucleus and the effect of emerin deficiency. *Biophysical Journal.* **91** (12), 4649-4664 (2006).

28. Davidson, P. M. et al. High-throughput microfluidic micropipette aspiration device to probe time-scale dependent nuclear mechanics in intact cells. *Lab on a Chip.* **19** (21), 3652-3663 (2019).

29. Lombardi, M., Zwerger, M., Lammerding, J. Biophysical assays to probe the mechanical properties of the interphase cell nucleus: Substrate strain application and microneedle manipulation. *Journal of Visualized Experiments: JoVE.* (55), 3-9 (2011).

30. Luo, T., Mohan, K., Iglesias, P. A., Robinson, D. N. Molecular mechanisms of cellular mechanosensing. *Nature Materials.* **12** (11), 1064-1071 (2013).

31. Dahl, K. N., Engler, A. J., Pajerowski, J. D., Discher, D. E. Power-law rheology of isolated nuclei with deformation mapping of nuclear substructures. *Biophysical Journal.* **89** (4), 2855-2864 (2005).

32. Guilluy, C. et al. Isolated nuclei adapt to force and reveal a mechanotransduction pathway in the nucleus. *Nature Cell Biology.* **16** (4), 376-381 (2014).

33. Bustamante, C. J., Wang, M. D. Optical tweezers in single-molecule biophysics. *Nature Reviews Methods Primers.* 1-29 (2021).

34. Svoboda, K., Block, S. M. Force and velocity measured for single kinesin molecules. *Cell.* **77** (5), 773-784 (1994).

35. Berg-Sørensen, K., Flyvbjerg, H. Power spectrum analysis for optical tweezers. *Review of Scientific Instruments.* **75** (3), 594-612 (2004).

36. Smith, S. B., Cui, Y., Bustamante, C. Optical-trap force transducer that operates by direct measurement of light momentum. *Methods in Enzymology.* **361** (1994), 134-162 (2003).

37. Farré, A., Montes-Usategui, M. A force detection technique for single-beam optical traps based on direct measurement of light momentum changes. *Optics Express.* **18** (11), 11955 (2010).

38. Català, F., Marsà, F., Montes-Usategui, M., Farré, A., Martín-Badosa, E. Extending calibration-free force measurements to optically-trapped rod-shaped samples. *Scientific Reports.* **7** (January), 1-10 (2017).

39. Bui, A. A. M. et al. Calibration of force detection for arbitrarily shaped particles in optical tweezers. *Scientific Reports.* **8** (1), 1-12 (2018).

40. Farré, A., Marsà, F., Montes-Usategui, M. Beyond the hookean spring model: Direct measurement of optical forces through light momentum changes. *Methods in Molecular Biology.* **1486** (2017).

41. Farré, A., Marsà, F., Montes-Usategui, M. Optimized back-focal-plane interferometry directly measures forces of optically trapped particles. *Optics Express.* **20** (11), 12270 (2012).

42. Jun, Y., Tripathy, S. K., Narayanareddy, B. R. J., Mattson-Hoss, M. K., Gross, S. P. Calibration of optical tweezers for in vivo force measurements: How do different approaches compare? *Biophysical Journal.* **107** (6), 1474-1484 (2014).

43. Mas, J., Farré, A., Sancho-Parramon, J., Martín-Badosa, E., Montes-Usategui, M. Force measurements with optical tweezers inside living cells. *Optical Trapping and Optical Micromanipulation XI.* **9164**, 91640U (2014).

44. Schürmann, M., Scholze, J., Müller, P., Guck, J., Chan, C. J. Cell nuclei have lower refractive index and mass density than cytoplasm. *Journal of Biophotonics.* **9** (10), 1068-1076 (2016).

45. Rosen, J. N., Sweeney, M. F., Mably, J. D. Microinjection of zebrafish embryos to analyze gene function. *Journal of Visualized Experiments: JoVE.* (25), 1-5 (2009).

46. Westerfield, M. *The Zebrafish Book. A Guide for the Laboratory Use of Zebrafish.* (Danio rerio), 5th Edition. University of Oregon Press, Eugene (Book) (2007).

47. Schubert, R. et al. Assay for characterizing the recovery of vertebrate cells for adhesion measurements by single-cell force spectroscopy. *FEBS Letters.* **588** (19), 3639-3648 (2014).

48. Koschwanez, J. H., Carlson, R. H., Meldrum, D. R. Thin PDMS films using long spin times or tert-butyl alcohol as a solvent. *PLoS One.* **4** (2), 2-6 (2009).

49. Das, R. et al. An asymmetric mechanical code ciphers curvature-dependent proprioceptor activity. *Science Advances.* **7**, eabg4617 (2021).

50. Chardès, C., Clement, R., Blanc, O., Lenne, P. F. Probing cell mechanics with bead-free optical tweezers in the drosophila embryo. *Journal of Visualized Experiments: JoVE.* **2018** (141), 1-11 (2018).

51. Staunton, J. R., Blehm, B., Devine, A., Tanner, K. In situ calibration of position detection in an optical trap for active microrheology in viscous materials. *Optics Express.* **25** (3), 1746 (2017).

52. Bola, R., Treptow, D., Marzoa, A., Montes-Usategui, M., Martin-Badosa, E. Acousto-holographic optical tweezers. *Optics Letters.* **45** (10), 2938-2941 (2020).

53. Thalhammer, G., Obmascher, L., Ritsch-Marte, M. Direct measurement of axial optical forces. *Optics Express.* **23** (5), 6112 (2015).

54. Vermeulen, K. C. et al. Calibrating bead displacements in optical tweezers using acousto-optic deflectors. *Review of Scientific Instruments.* **77** (1), 1-6 (2006).

55. Dzementsei, A., Barooji, Y. F., Ober, E. A., Oddershede, L. B. Foregut organ progenitors and their niche display distinct viscoelastic properties in vivo during early morphogenesis stages. *bioRxiv.* 1-35 (2021).

56. Behrndt, M. et al. Forces driving epithelial spreading in zebrafish gastrulation. *Science.* **338** (6104), 257-260 (2012).

57. Krieg, M. et al. Atomic force microscopy-based mechanobiology. *Nature Reviews Physics.* (2018).

58. A-Hassan, E. et al. Relative microelastic mapping of living cells by atomic force microscopy. *Biophysical Journal.* **74** (3), 1564-1578 (1998).

59. Khalilgharibi, N. et al. Stress relaxation in epithelial monolayers is controlled by the actomyosin cortex. *Nature Physics.* **15** (2019).

60. Crick, S. L., Yin, F. C. Assessing micromechanical properties of cells with atomic force microscopy: importance of the contact point. *Biomechanics and Modeling in Mechanobiology.* **6** (3), 199-210 (2007).

61. Hurst, S., Vos, B. E., Betz, T. Intracellular softening and fluidification reveals a mechanical switch of cytoskeletal material contributions during division. *bioRxiv.* 2021.01.07.425761 (2021).

62. Kaplan, J. L., Bonfanti, A., Kabla, A. RHEOS.jl - A Julia package for rheology data analysis. *arXiv.* **4**, 1-5 (2020).

63. Bonfanti, A., Kaplan, J. L., Charras, G., Kabla, A. Fractional viscoelastic models for power-law materials. *Soft Matter.* **16** (26), 6002-6020 (2020).

64. Rivas-Barbosa, R., Escobedo-Sánchez, M. A., Tassieri, M., Laurati, M. i-Rheo: determining the linear viscoelastic moduli of colloidal dispersions from step-stress measurements. *Physical Chemistry Chemical Physics: PCCP.* **22** (7), 3839-3848 (2020).

65. Tassieri, M. et al. i-Rheo: Measuring the materials' linear viscoelastic properties "in a step "! *Journal of Rheology.* **60** (4), 649-660 (2016).

66. Zhong, M. C., Wei, X. Bin, Zhou, J. H., Wang, Z. Q., Li, Y. M. Trapping red blood cells in living animals using optical tweezers. *Nature Communications.* **4**, 1767-1768 (2013).

67. Harlepp, S., Thalmann, F., Follain, G., Goetz, J. G. Hemodynamic forces can be accurately measured in vivo with optical tweezers. *Molecular Biology of the Cell.* **28** (23), 3252-3260 (2017).

68. Bayoudh, S., Mehta, M., Rubinsztein-Dunlop, H., Heckenberg, N. R., Critchley, C. Micromanipulation of chloroplasts using optical tweezers. *Journal of Microscopy.* **203** (2), 214-222 (2001).

69. Favre-Bulle, I. A., Stilgoe, A. B., Rubinsztein-Dunlop, H., Scott, E. K. Optical trapping of otoliths drives vestibular behaviours in larval zebrafish. *Nature Communications.* **8** (1), 630 (2017).

70. Bambardekar, K., Clément, R., Blanc, O., Chardès, C., Lenne, P. F. Direct laser manipulation reveals the mechanics of cell contacts in vivo. *Proceedings of the National Academy of Sciences of the United States of America.* **112** (5), 1416-1421 (2015).

71. Ferro, V., Chuai, M., McGloin, D., Weijer, C. J. Measurement of junctional tension in epithelial cells at the onset of primitive streak formation in the chick embryo via non-destructive optical manipulation. *Development (Cambridge).* **147** (3) (2020).

72. Hörner, F. et al. Holographic optical tweezers-based in vivo manipulations in zebrafish embryos. *Journal of Biophotonics.* **10** (11), 1492-1501 (2017).

73. Zhong, M.-C., Wang, Z.-Q., Li, Y.-M. Aberration compensation for optical trapping of cells within living mice. *Applied Optics.* **56** (7), 1972 (2017).

74. Català, F., Marsà, F., Montes-Usategui, M., Farré, A., Martín-Badosa, E. Influence of experimental parameters on the laser heating of an optical trap. *Scientific Reports.* **7** (1), 1-9 (2017).

75. Taylor, M. A., Waleed, M., Stilgoe, A. B., Rubinsztein-Dunlop, H., Bowen, W. P. Enhanced optical trapping via structured scattering. *Nature Photonics.* **9** (10), 669-673 (2015).

76. Bormuth, V. et al. Optical trapping of coated microspheres. *Optics Express.* **16** (18), 13831-13844 (2008).

77. Sudhakar, S. et al. Germanium nanospheres for ultraresolution picotensiometry of kinesin motors. *Science.* **371** (6530), eabd9944 (2021).

78. Shan, X. et al. Optical tweezers beyond refractive index mismatch using highly doped upconversion nanoparticles. *Nature Nanotechnology.* 16 (5), 531-537 (2021).